

Fighting Hallucinations with Counterfactuals: Diffusion-Guided Perturbations for LVLMM Hallucination Suppression

Hamidreza Dastmalchi
York University
Toronto, Canada
hrd@yorku.ca

Aijun An
York University
Toronto, Canada
aan@yorku.ca

Ali Cheraghian
Macquarie University
Sydney, Australia
ali.cheraghian@mq.edu.au

Hamed Barzamini
Northern Illinois University
Illinois, USA
h.barzamini@niu.edu

Abstract

While large vision–language models (LVLMMs) achieve strong performance on multimodal tasks, they frequently generate hallucinations—unfaithful outputs misaligned with the visual input. To address this issue, we introduce CIPHER (Counterfactual Image Perturbations for Hallucination Extraction and Removal), a training-free method that suppresses vision-induced hallucinations via lightweight feature-level correction. Unlike prior training-free approaches that primarily focus on text-induced hallucinations, CIPHER explicitly targets hallucinations arising from the visual modality. CIPHER operates in two phases. In the offline phase, we construct OHC-25K (Object-Hallucinated Counterfactuals, 25,000 samples), a counterfactual dataset consisting of diffusion-edited images that intentionally contradict the original ground-truth captions. We pair these edited images with the unchanged ground-truth captions and process them through an LVLMM to extract hallucination-related representations. Contrasting these representations with those from authentic (image, caption) pairs reveals structured, systematic shifts spanning a low-rank subspace characterizing vision-induced hallucination. In the inference phase, CIPHER suppresses hallucinations by projecting intermediate hidden states away from this subspace. Experiments across multiple benchmarks show that CIPHER significantly reduces hallucination rates while preserving task performance, demonstrating the effectiveness of counterfactual visual perturbations for improving LVLMM faithfulness. Code and additional materials are available at <https://hamidreza-dastmalchi.github.io/cipher-cvpr2026/>.

1. Introduction

Large vision-language models (LVLMMs) commonly integrate vision encoders with pretrained large language models (LLMs) via lightweight connector modules, enabling joint

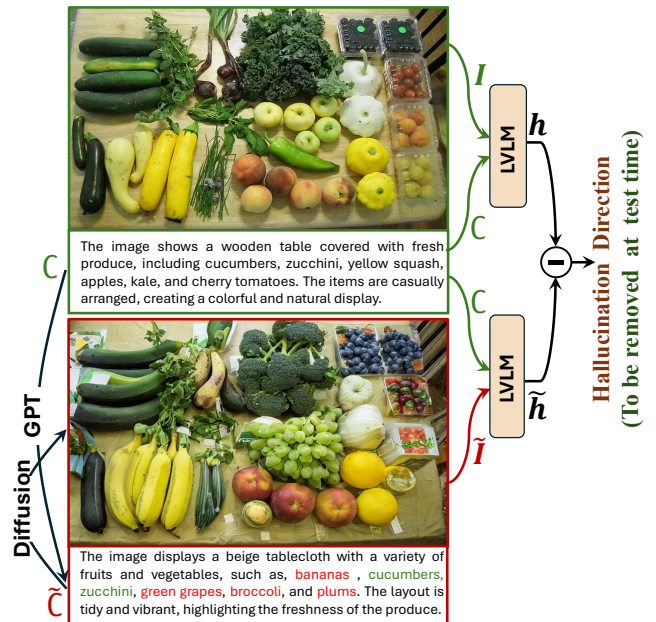


Figure 1. Given an image–caption pair (I, C) , we generate a counterfactual image \tilde{I} using a diffusion model conditioned on a GPT-perturbed caption \tilde{C} via controlled perturbations. A vision–language model encodes both (I, C) and (\tilde{I}, \tilde{C}) , yielding features h and \tilde{h} . Their difference $\delta = \tilde{h} - h$ captures the hallucination direction we later nullify at inference.

reasoning over visual and textual inputs. This modular design underpins models like MiniGPT-4 [43], LLaVA [24, 25], and mPLUG-Owl2 [38, 39], which are further refined through instruction tuning on multimodal datasets.

While LVLMMs show remarkable capabilities, they often suffer from *hallucination*, generating descriptions of objects, attributes, or scenes not present in the input image. Different studies have explored the roots of hallucination [4, 26], showing that it arises not only from the generative tendencies of LLMs but also from weak vision grounding, modality misalignment, biased training data, and context-blind decoding strategies.

Hallucination mitigation in LVLMs generally falls into three categories. (1) *Training-based* methods improve visual grounding through additional supervision or objective design but require costly annotations, retraining, or architectural changes [8, 13, 16, 22, 23, 41]. (2) *Post-processing* methods detect and revise hallucinations after generation using external tools [40, 42]. (3) *Test-time* techniques are lightweight strategies applied during inference that adapt internal representations or the decoding process without requiring retraining or modifying model parameters [14, 17, 27, 35]. Although effective, some test-time approaches, including contrastive decoding, require multiple forward passes [17], leading to higher inference cost. In contrast, test-time feature-level intervention techniques are more efficient, requiring only a single forward pass [35]. However, existing methods predominantly target hallucinations arising from the language component, leaving vision-induced hallucinations comparatively underexplored. In this work, we instead focus on hallucinations rooted in the visual modality by generating counterfactual images to extract and subsequently remove hallucination directions.

To this end, we propose CIPHER (Counterfactual Image Perturbations for Hallucination Extraction and Removal), a training-free, test-time hallucination mitigation method that performs feature-level intervention to address hallucinations in LVLMs. In the offline phase, we construct OHC-25K (Object Hallucination Counterfactuals), a 25K-sample diffusion-edited counterfactual dataset created from a subset of image–caption pairs from MSCOCO [21]. Figure 1 illustrates how counterfactual images are generated from ground-truth image–caption pairs and incorporated into our framework. We first perturb each caption using the GPT-3.5 model [6], then apply a partial forward diffusion process to the image, and run the reverse diffusion process conditioned on the altered caption to synthesize a hallucinated variant. This controlled editing preserves the global structure of the original image while injecting semantically incorrect yet visually plausible elements (e.g., adding a cluster of grapes that are not present in the scene). We feed both the ground-truth and diffusion-edited image–caption pairs through the LVM to extract hidden representations, compute their difference vectors, and stack them into a matrix. Applying Singular Value Decomposition (SVD) to these vectors reveals a low-rank subspace capturing the dominant directions of vision-induced hallucinations. At inference time, CIPHER suppresses hallucinations by projecting intermediate hidden representations away from this subspace, without modifying model weights or requiring any additional training.

We conduct extensive experiments across multiple benchmarks to evaluate our approach. Results demonstrate that it effectively mitigates hallucinations without degrading the overall performance of LVLMs on tasks such as image captioning and visual question answering. Unlike many

existing methods, our solution operates entirely at test time and introduces no inference-time overhead, as hallucination suppression is achieved via a lightweight projection on intermediate hidden states. To the best of our knowledge, this is the first method to identify hallucination directions in the feature space by hallucinating images, enabling more targeted mitigation of vision-induced hallucinations. Our main contributions are as follows:

(1) We present **CIPHER**, a training-free test-time hallucination mitigation method that specifically targets hallucinations arising from the visual modality. (2) We develop a diffusion-guided procedure to construct **OHC-25K**, a counterfactual dataset of diffusion-edited images whose semantics intentionally contradict their ground-truth captions. These counterfactual pairs enable us to estimate a hallucination subspace by contrasting them with clean image–caption representations. (3) During inference, we mitigate hallucinations by projecting hidden representations onto the orthogonal complement of the estimated subspace, without requiring model retraining or parameter updates. (4) Extensive experiments across multiple benchmarks demonstrate that CIPHER reduces hallucinations while preserving the overall quality of multimodal generation.

2. Related Work

2.1. Large Vision-Language Models (LVLMs)

The success of large language models (LLMs) [5, 11, 32] has paved the way for large vision-language models (LVLMs), which extend language understanding to visual inputs. By integrating vision encoders with LLMs via adaptation modules and instruction tuning, LVLMs such as mPLUG-Owl2 [39], Flamingo [1], BLIP-2 [18], LLaVA [24], and MiniGPT-4 [43] achieve strong performance on tasks like image captioning, visual question answering, and multimodal dialogue. However, they remain susceptible to hallucination, limiting robustness in real-world settings.

2.2. Hallucination Mitigation in LVLMs

To mitigate hallucinations in LVLMs, various approaches have been proposed across the training, inference, and post-processing stages. While training-based methods [3, 13, 16, 22, 34, 37] are often effective, they typically require expensive annotations, model retraining, or architectural modifications, limiting their scalability in practice. In contrast, post-processing strategies mitigate hallucinations without altering the base model, typically by detecting and revising errors after generation using heuristics or external tools [40, 42]. However, dependence on auxiliary models limits generalizability and complicates deployment. Test-time approaches [9, 15, 27] address these limitations by intervening directly during inference, offering a more efficient solution.

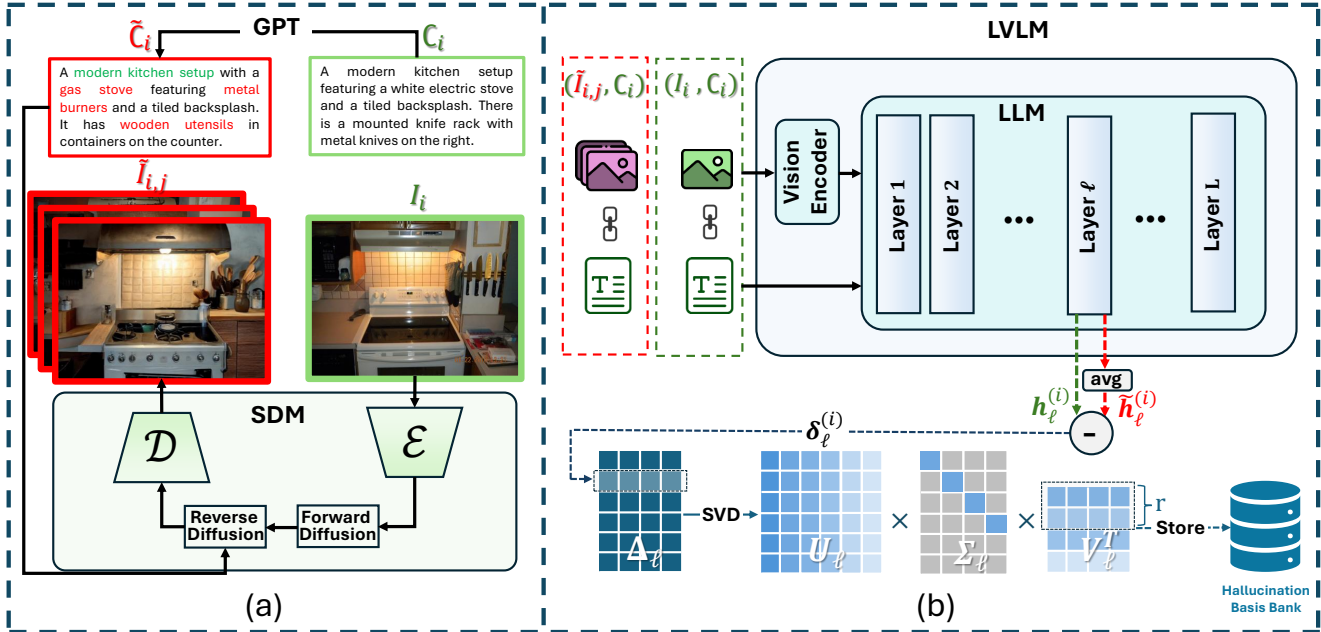


Figure 2. (a) Hallucinated image generation: given an image I_i and its ground-truth caption C_i , a GPT model generates a hallucinated caption \tilde{C}_i . The image is then encoded by the encoder \mathcal{E} of the Stable Diffusion Model (SDM), and both forward and reverse diffusion steps are applied, conditioned on \tilde{C}_i , to produce hallucinated images $\tilde{I}_{i,j}$. (b) Estimating hallucination subspace: the LVLM encodes both hallucinated and ground-truth image-caption pairs to extract hidden states. Feature differences $\{\delta_\ell^{(i)}\}_{i=1}^M$ are computed, stacked, and decomposed via SVD. The top r right-singular vectors are retained in a hallucination basis bank for inference-time suppression.

2.3. Test-time Hallucination Suppression in LVLMS

Test-time hallucination mitigation methods intervene during inference to improve factual alignment without modifying the model parameters. These include decoding-based techniques [2, 14, 15, 17, 36, 44], which steer generation by adjusting sampling distributions or applying constraints to suppress hallucinations. While effective, these approaches often involve multiple forward passes, leading to increased inference-time overhead. In contrast, feature-level interventions provide a more efficient solution. These methods operate by modifying internal representations within a single forward pass, guiding the model away from hallucinated outputs [7, 19, 27, 33, 35]. For example, Nullu [35] extract hallucination directions by contrasting features from textually perturbed inputs and shift the model’s hidden states accordingly. However, these approaches mostly focus on language-induced hallucinations, overlooking those rooted in the visual modality. CIPHER fills this gap by perturbing images with a diffusion model to extract the hallucination subspace and suppress it via feature projection.

3. Method

CIPHER estimates feature directions triggered by hallucination-inducing visual cues and suppresses these components during inference. The method operates in

two stages: (1) an *offline phase*, where we construct a counterfactual dataset and estimate the hallucination subspaces; and (2) an *inference phase*, where we nullify hallucination-prone components in hidden representations during generation.

3.1. Offline Phase

Counterfactual Dataset Generation (OHC-25K). To reveal hallucination-sensitive directions in the LVLM’s feature space, we construct a dataset of *counterfactual image-caption pairs* in which the visual content is structurally preserved but semantically altered.

Figure 2(a) illustrates how the counterfactual images are generated. We begin with $M = 5,000$ randomly selected image-caption pairs from the MSCOCO training set, $\{(I_i, C_i)\}_{i=1}^M$. Following LURE [42], we generate a hallucinated caption \tilde{C}_i (displayed with a red border) for each ground-truth caption C_i (displayed with a green border) using a GPT-based perturbation that injects plausible but incorrect objects.

Next, each image I_i is encoded into the latent space of Stable Diffusion Model (SDM) [30] using its VAE encoder:

$$z_0 = \mathcal{E}(I_i). \quad (1)$$

We then apply t_h steps of the forward diffusion process to introduce Gaussian noise. Let $\bar{\alpha}_{t_h}$ denote the cumulative

product of noise scheduling coefficients up to step t_h . The partially noised latent is given by:

$$\tilde{z}_{t_h} = \sqrt{\alpha_{t_h}} z_0 + \sqrt{1 - \alpha_{t_h}} \epsilon, \quad \epsilon \sim \mathcal{N}(0, I). \quad (2)$$

To simulate semantic hallucination, we reverse-denoise \tilde{z}_{t_h} while conditioning on the hallucinated caption:

$$\tilde{z}_{t-1} = f_\theta(\tilde{z}_t, t, \tilde{C}_i), \quad t = t_h, \dots, 1. \quad (3)$$

Decoding the final denoised latent (\tilde{z}_0) yields a counterfactual image:

$$\tilde{I}_{i,j} = \mathcal{D}(\tilde{z}_0), \quad (4)$$

where $j = 1, \dots, B$ indexes the B counterfactual variants generated from different Gaussian noise seeds (we use $B = 5$). Pairing each counterfactual image with the original ground-truth caption creates a semantic conflict while preserving structural alignment. This forms the *Object-Hallucination Counterfactuals* dataset, constructed from $M = 5,000$ image-caption pairs with $B = 5$ counterfactual variants per image, resulting in 25,000 images.

$$\text{OHC-25K} = \{(\tilde{I}_{i,j}, C_i) \mid i = 1, \dots, M, j = 1, \dots, B\}. \quad (5)$$

Estimating the Hallucination Subspace. Figure 2(b) illustrates how the hallucination subspace is extracted. For each original pair (I_i, C_i) and its B counterfactual variants $(\tilde{I}_{i,j}, C_i)$, we extract hidden representations from the frozen LLM. Let $\mathbf{h}_{\ell,k}^{(i)} \in \mathbb{R}^d$ denote the hidden state of the k -th caption token at layer ℓ for the original pair, and $\tilde{\mathbf{h}}_{\ell,k}^{(i,j)} \in \mathbb{R}^d$ for the j -th counterfactual variant. We mean-pool across caption tokens:

$$\mathbf{h}_\ell^{(i)} = \frac{1}{N} \sum_{k=1}^N \mathbf{h}_{\ell,k}^{(i)}, \quad \tilde{\mathbf{h}}_\ell^{(i,j)} = \frac{1}{N} \sum_{k=1}^N \tilde{\mathbf{h}}_{\ell,k}^{(i,j)}. \quad (6)$$

Since each image yields B hallucinated samples, we compute the aggregated counterfactual representation as:

$$\tilde{\mathbf{h}}_\ell^{(i)} = \frac{1}{B} \sum_{j=1}^B \tilde{\mathbf{h}}_\ell^{(i,j)}. \quad (7)$$

The hallucination direction for sample i at layer ℓ is defined as $\delta_\ell^{(i)} = \tilde{\mathbf{h}}_\ell^{(i)} - \mathbf{h}_\ell^{(i)}$. Stacking these directions across all samples yields:

$$\Delta_\ell = [\delta_\ell^{(1)}; \delta_\ell^{(2)}; \dots; \delta_\ell^{(M)}] \in \mathbb{R}^{M \times d}. \quad (8)$$

We apply Singular Value Decomposition (SVD) to the stacked difference matrix to identify the principal hallucination directions:

$$\Delta_\ell = \mathbf{U}_\ell \Sigma_\ell \mathbf{V}_\ell^\top. \quad (9)$$

The top r right-singular vectors $\mathbf{V}_{\ell,r} = [\mathbf{v}_{\ell,1}, \dots, \mathbf{v}_{\ell,r}]$ span the hallucination subspace at layer ℓ . These vectors form our *hallucination basis bank*.

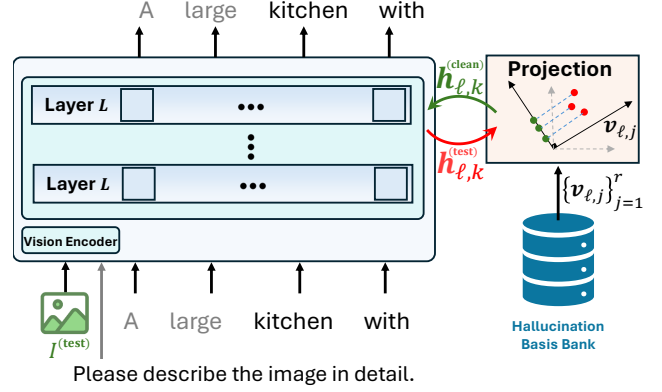


Figure 3. Inference-time projection mechanism. Given an input image and instruction, the model generates text autoregressively. At each decoding step during generation, hidden states from selected layers are projected onto the subspace orthogonal to the corresponding hallucination space, using the hallucination basis bank obtained in the offline phase.

3.2. Inference Phase

Test-Time Nullification. The hallucination nullification process during test time is illustrated in Figure 3. At each decoding step k and selected layer ℓ , the hidden state of the test image during inference is denoted by $\mathbf{h}_{\ell,k}^{\text{test}} \in \mathbb{R}^d$. To suppress hallucinations, we remove components aligned with the hallucination subspace:

$$\mathbf{h}_{\ell,k}^{\text{clean}} = \mathbf{h}_{\ell,k}^{\text{test}} - \sum_{j=1}^r \langle \mathbf{h}_{\ell,k}^{\text{test}}, \mathbf{v}_{\ell,j} \rangle \mathbf{v}_{\ell,j}. \quad (10)$$

Equivalently, this operation can be expressed using the projection matrix $\mathbf{P}_\ell = \mathbf{I} - \mathbf{V}_{\ell,r} \mathbf{V}_{\ell,r}^\top$, which yields:

$$\mathbf{h}_{\ell,k}^{\text{clean}} = \mathbf{P}_\ell \mathbf{h}_{\ell,k}^{\text{test}}. \quad (11)$$

This layer-wise nullification is applied before decoding each token, removing hallucination-prone directions while preserving core semantics.

4. Experiments

4.1. Implementation Details

We evaluate CIPHER on CHAIR [29] and Offline POPE (OPOPE) [9] using LLaVA-1.5 [24] with Vicuna [10], MiniGPT-4 [43] with LLaMA2 [32], and mPLUG-Owl2 [39]. For decoding, we use a beam size of 3, setting the maximum number of generated tokens to 64 for CHAIR and 256 for OPOPE. The hallucination subspace is constructed using the top r singular vectors, with $r = 8$ for LLaVA, 64 for MiniGPT-4, and 32 for mPLUG-Owl2, selected via grid search. Following [35], we apply the projection at upper layers (16–32). Visual hallucinations are

Method	LLaVA-1.5			MiniGPT-4			mPLUG-Owl2		
	CHAIR _S ↓	CHAIR _I ↓	BLEU ↑	CHAIR _S ↓	CHAIR _I ↓	BLEU ↑	CHAIR _S ↓	CHAIR _I ↓	BLEU ↑
Greedy	20.40 \pm 2.80	7.08 \pm 0.33	15.72 \pm 0.10	32.40 \pm 2.20	12.20 \pm 0.42	14.57 \pm 0.11	22.90 \pm 0.90	8.62 \pm 0.11	15.01 \pm 0.24
Beam Search	19.50 \pm 2.30	6.84 \pm 0.79	15.99 \pm 0.14	30.10 \pm 0.30	11.87 \pm 0.37	15.35 \pm 0.24	20.30 \pm 0.70	7.62 \pm 0.19	15.43 \pm 0.05
DoLa (ICLR'24)	20.20 \pm 2.80	6.75 \pm 0.54	15.68 \pm 0.10	31.90 \pm 3.30	12.15 \pm 0.89	14.54 \pm 0.12	22.40 \pm 1.80	8.36 \pm 0.04	15.13 \pm 0.21
OPERA (CVPR'24)	17.50 \pm 0.50	6.07 \pm 0.32	16.02 \pm 0.02	29.70 \pm 0.30	11.96 \pm 0.29	14.82 \pm 0.05	20.07 \pm 2.07	7.18 \pm 0.39	15.41 \pm 0.12
VCD (CVPR'24)	20.30 \pm 1.10	7.28 \pm 0.10	14.53 \pm 0.01	29.00 \pm 2.80	12.64 \pm 1.19	14.42 \pm 0.01	22.80 \pm 0.80	8.68 \pm 0.17	15.14 \pm 0.13
Woodpecker (SCIS'24)	23.85 \pm 4.62	7.50 \pm 0.01	17.05 \pm 0.00	28.87 \pm 2.20	10.20 \pm 0.85	15.30 \pm 0.01	26.33 \pm 1.98	8.43 \pm 0.80	16.43 \pm 0.00
LURE (ICLR'24)	19.48 \pm 2.35	6.50 \pm 0.38	15.97 \pm 0.01	27.88 \pm 2.25	10.20 \pm 0.85	15.03 \pm 0.01	21.27 \pm 0.06	7.67 \pm 0.16	15.65 \pm 0.15
HALC (ICML'24)	16.90 \pm 2.10	5.72 \pm 0.55	16.02 \pm 0.04	25.20 \pm 2.00	9.42 \pm 0.41	14.91 \pm 0.13	18.80 \pm 1.20	7.00 \pm 0.01	15.33 \pm 0.24
Nullu (CVPR'25)	15.20 \pm 0.60	5.30 \pm 0.03	15.69 \pm 0.04	21.40 \pm 1.00	8.99 \pm 0.36	14.81 \pm 0.06	15.60 \pm 1.20	5.77 \pm 0.01	15.45 \pm 0.01
CIPHER (Ours)	13.05 \pm 0.57	4.53 \pm 0.38	15.82 \pm 0.25	18.48 \pm 1.20	8.33 \pm 0.17	15.10 \pm 0.43	13.60 \pm 1.06	4.92 \pm 0.15	16.25 \pm 0.47

Table 1. CHAIR and BLEU scores across LVLMS; lower CHAIR = less hallucination, higher BLEU = better fluency.

generated using Stable Diffusion v1.5, with noise added up to $t_h = 0.5T$, where T denotes the total number of diffusion steps. We use a classifier-free guidance scale of 7.5. See the Appendix for additional details.

4.2. Datasets and Benchmarks

For the offline phase, we follow LURE [42] using 5,000 image-caption pairs from the MSCOCO training split [21]. For evaluation, we follow established evaluation protocols [14, 40] and randomly sample 500 images from the MSCOCO validation set using the widely adopted CHAIR and POPE metrics. We report mean and standard deviation over three runs with different random seeds.

CHAIR. We use the CHAIR benchmark [29] to evaluate object hallucination in generated image descriptions. CHAIR_S measures the percentage of sentences that contain at least one hallucinated object, while CHAIR_I captures the proportion of hallucinated objects among all generated object mentions. We also report BLEU [28] to evaluate text quality and confirm that fluency is preserved.

OPOPE. We evaluate object hallucination using the Offline POPE [20], which includes three negative sampling strategies: random, popular, and adversarial. We adopt the OPOPE protocol [9], which applies a CHAIR-style captioning setup and modifies the evaluation metric to detect the inclusion of negative objects in generated captions.

MMHAL-Bench. MMHal [31] evaluates LVLMS across eight hallucination types, including attributes, adversarial objects, comparisons, counting, relations, environment, holistic descriptions, and others, providing a broad assessment beyond object-level errors. We measure the response informativeness using GPT-4.

LLaVA-Bench. We also evaluate on LLaVA-Bench [25], a curated benchmark of 24 diverse images with human-written descriptions and targeted questions. It assesses accuracy and detailedness, complementing CHAIR and

POPE. Following [17, 40], we use GPT-4V to compare original and edited responses based on their alignment with the image and question.

4.3. Baselines

We compare CIPHER with state-of-the-art hallucination mitigation methods, categorized as test-time approaches and post-processing strategies. Test-time methods include DoLa [12], VCD [17], HALC [9], OPERA [14], and Nullu [35]. The first four apply decoding-based interventions, while Nullu projects hidden representations onto a hallucination-free subspace. Post-processing methods Woodpecker [40] and LURE [42] detect and rewrite hallucinated spans using external models.

4.4. Results on CHAIR

We prompt all methods with the instruction: “Please describe this image in detail” and report the results in Table 1. CIPHER consistently achieves the lowest hallucination rates across all three vision-language models (LLaVA-1.5, MiniGPT-4, and mPLUG-Owl2). For example, on LLaVA-1.5, CIPHER reduces CHAIR_S to 13.05%, which is a 2.15% absolute improvement over the second-best model (Nullu at 15.20%), and a 7.35% drop compared to the original greedy baseline (20.40%). On MiniGPT-4, CIPHER further brings CHAIR_S down to 18.48%, improving upon Nullu by 2.92% and reducing hallucinations by a substantial 13.92% relative to the greedy baseline (32.40%). Similarly, for mPLUG-Owl2, CIPHER scores 13.60% on CHAIR_S, which is 2.00% better than the second-best model and 9.30% better than the original model. These gains in CHAIR_S are mirrored in CHAIR_I as well, with CIPHER consistently outperforming all baselines in object-level hallucination. Importantly, CIPHER maintains or improves BLEU scores across all models, indicating effective hallucination mitigation without sacrificing generation richness.

Method	LLaVA-1.5			MiniGPT-4			mPLUG-Owl2		
	Accuracy \uparrow	Precision \uparrow	F score \uparrow	Accuracy \uparrow	Precision \uparrow	F score \uparrow	Accuracy \uparrow	Precision \uparrow	F score \uparrow
Greedy	79.14 \pm 0.89	91.98 \pm 0.82	90.45 \pm 0.86	71.22 \pm 1.27	93.72 \pm 1.02	90.04 \pm 1.23	76.46 \pm 0.92	88.85 \pm 1.15	87.29 \pm 1.15
Beam Search	79.41 \pm 0.69	92.52 \pm 0.55	90.96 \pm 0.59	71.65 \pm 1.15	94.70 \pm 0.60	90.97 \pm 0.85	76.76 \pm 1.02	90.28 \pm 0.80	88.56 \pm 0.87
DoLa (ICLR'24)	78.98 \pm 0.56	91.66 \pm 0.81	90.15 \pm 0.79	71.28 \pm 1.15	93.92 \pm 0.83	90.22 \pm 1.04	76.07 \pm 1.09	88.54 \pm 1.25	86.95 \pm 1.27
OPERA (CVPR'24)	79.29 \pm 0.32	92.25 \pm 0.07	90.71 \pm 0.11	70.48 \pm 1.63	94.41 \pm 1.11	90.66 \pm 1.42	75.49 \pm 1.29	91.23 \pm 1.06	89.11 \pm 1.17
VCD (CVPR'24)	78.01 \pm 0.75	91.33 \pm 0.88	89.69 \pm 0.89	70.83 \pm 1.83	92.31 \pm 0.88	88.76 \pm 1.29	75.49 \pm 1.27	88.75 \pm 1.56	87.02 \pm 1.57
HALC (ICML'24)	77.87 \pm 0.22	93.17 \pm 0.39	91.25 \pm 0.38	71.17 \pm 0.89	94.88 \pm 0.15	90.95 \pm 0.42	74.93 \pm 1.09	90.20 \pm 0.90	88.12 \pm 0.99
Nullu (CVPR'25)	79.52 \pm 0.04	93.46 \pm 0.03	91.79 \pm 0.04	71.92 \pm 0.39	95.96 \pm 0.65	92.07 \pm 0.65	77.09 \pm 1.37	92.83 \pm 0.29	90.80 \pm 0.52
CIPHER (Ours)	80.05\pm0.07	93.72\pm0.14	92.11\pm0.11	72.25\pm0.26	96.50\pm0.19	92.58\pm0.20	77.87\pm0.21	92.93\pm0.26	90.95\pm0.59

Table 2. Accuracy, precision, and F1 scores of different methods on the OPOPE benchmark, evaluated across LLaVA-1.5, MiniGPT-4, and mPLUG-Owl2.

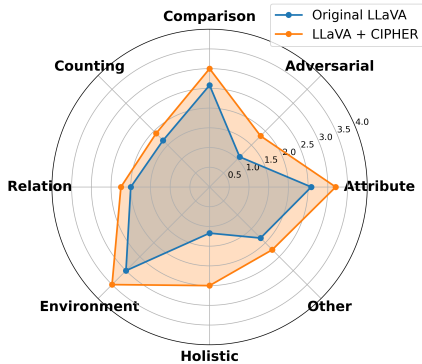


Figure 4. Radar chart of MMHal scores.

4.5. Results on OPOPE

As shown in Table 2, CIPHER achieves the highest scores across all three evaluation metrics for each model, clearly demonstrating its effectiveness in mitigating object hallucinations while preserving answer quality. The gains in precision are particularly pronounced relative to the unedited model, further highlighting CIPHER’s ability to suppress hallucinations while retaining relevant content. Despite the already saturated performance regime, CIPHER continues to deliver consistent improvements. Detailed POPE and OPOPE results are provided in the Appendix.

4.6. MMHal Benchmark Results

We evaluate hallucination reduction using the MMHal benchmark, which covers eight categories. This benchmark provides a fine-grained view of different hallucination types. As shown in Fig. 4, our LLaVA + CIPHER model achieves consistent improvements across all categories compared to the original LLaVA. The largest gains occur in *Attribute*, *Environment*, *Holistic* and *Adversarial* cases, while improvements in *Relation* and *Comparison*

Model	Method	Accuracy \uparrow	Detailedness \uparrow
LLaVA-1.5	Original	6.79 \pm 1.50	6.33 \pm 1.18
	CIPHER	7.08\pm1.32	6.75\pm1.13
MiniGPT-4	Original	5.54 \pm 2.41	5.58 \pm 2.06
	CIPHER	6.16\pm1.99	6.64\pm1.88
mPLUG-Owl2	Original	6.48 \pm 2.12	6.26 \pm 1.62
	CIPHER	7.35\pm1.63	6.91\pm1.61

Table 3. GPT-4V evaluations on LLaVA-Bench indicate that CIPHER consistently enhances model outputs, yielding higher accuracy and more detailed answers.

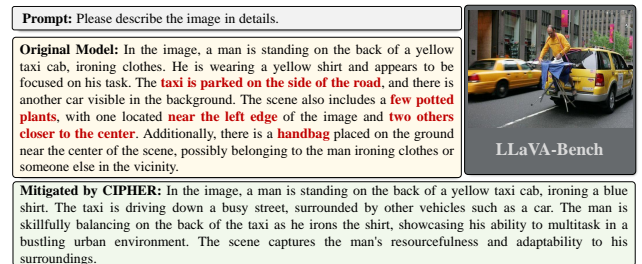


Figure 5. LLaVA-Bench example: CIPHER reduces hallucinations and improves grounding.

demonstrate enhanced global reasoning and grounding.

4.7. Evaluation on LLaVA-Bench

To further evaluate the effectiveness of our hallucination suppression strategy, we conduct quantitative and qualitative assessments on LLaVA-Bench [25]. GPT-4V is prompted to assign scores from 1 to 10 for both *accuracy* and *detailedness*, based on the input image, question, and model response (see Appendix for the prompt). As shown in Table 3, applying CIPHER consistently improves both

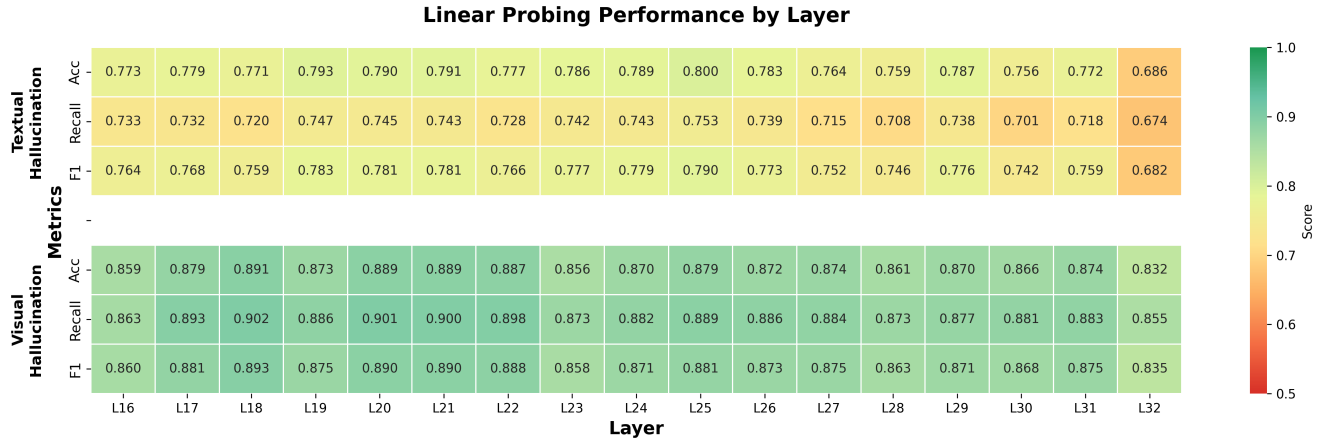


Figure 6. Layer-wise linear probing performance comparing textual and diffusion-based visual hallucination perturbations. Textual perturbations exhibit moderate and unstable separability across layers, whereas diffusion-based visual perturbations produce consistently high accuracy, recall, and F1.

metrics across all three models, reflecting enhanced visual grounding and reduced hallucination. We also present a qualitative case study using LLaVA-1.5-7B in Figure 5. The original model generates a caption that includes several hallucinated elements, such as “the taxi is parked,” “potted plants,” and a “handbag,” none of which are visible in the image. In contrast, the CIPHER-edited description accurately captures the scene—a man ironing a shirt on the back of a moving yellow taxi amidst traffic—without introducing spurious objects.

4.8. Inference Time

We evaluate the efficiency of various hallucination mitigation methods in terms of throughput, measured in items per second using LLaVA-7B on an NVIDIA A6000 GPU (Table 4). CIPHER matches the throughput of standard greedy decoding (0.70 items/s), substantially exceeding the efficiency of prior mitigation methods such as OPERA and HALC, which incur significant latency. In addition to its speed, CIPHER also achieves a much lower CHAIR_S score (13.05%), demonstrating superior hallucination suppression compared to all other baselines.

Metric	Greedy	Beam	DoLa	VCD	OPERA	HALC	Nullu	CIPHER
CHAIR _S ↓ (%)	20.40	19.50	20.20	20.30	17.50	16.90	15.20	13.05
Throughput ↑ (items/s)	0.70	0.55	0.42	0.35	0.10	0.05	0.70	0.70

Table 4. Comparison of CHAIR_S and throughput (items/s) for different mitigation methods, tested on LLaVA-7B with an NVIDIA A6000 GPU.

4.9. Ablation Studies

Linear Probing Analysis. To understand why the visual hallucination subspace is more effective than its text-based counterpart (Nullu method), we perform a layer-wise linear probing experiment. For each transformer layer, we train a logistic regression classifier to distinguish clean hidden representations from perturbed ones, using 400 samples for training and 1,000 samples for testing. We evaluate two perturbation types: (i) *textual hallucination*, where the clean image is paired with a GPT-generated hallucinated caption; and (ii) *visual hallucination*, where the caption remains unchanged but the image is perturbed using CIPHER-style diffusion counterfactuals.

As shown in Fig. 6, textual perturbations lead to only moderate separability (Accuracy: 0.73–0.80, F1: 0.74–0.78), with substantial variability across layers. This indicates that text-induced hallucination signals are relatively weak and noisy in the hidden representation space. In contrast, visual perturbations produce consistently high linear separability across all layers (Accuracy: 0.86–0.89, F1: 0.86–0.89). The diffusion counterfactuals introduce strong, structured, and layer-stable representation shifts that are easily captured by a linear classifier. These findings support our approach: the subspace derived from visual perturbations captures more meaningful hallucination directions, explaining CIPHER’s superior hallucination suppression.

Effect of Diffusion Time Step. We investigate how the strength of semantic perturbation, controlled by the diffusion timestep (t_h) impacts the quality of the hallucination subspace in CIPHER. To assess the impact of diffusion strength, we evaluate four timesteps $t_h \in \{0.25T, 0.5T, 0.75T, T\}$, where T is the maximum diffusion step. At each t_h , we perform a round-trip diffusion:

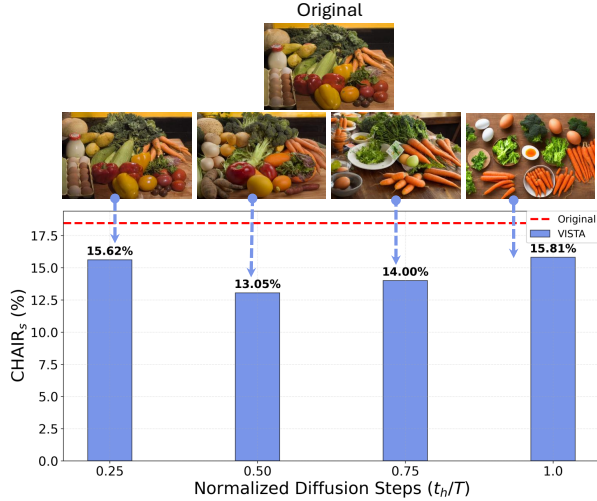


Figure 7. CHAIR_S of CIPHER using hallucination subspaces derived from images perturbed at different diffusion steps.

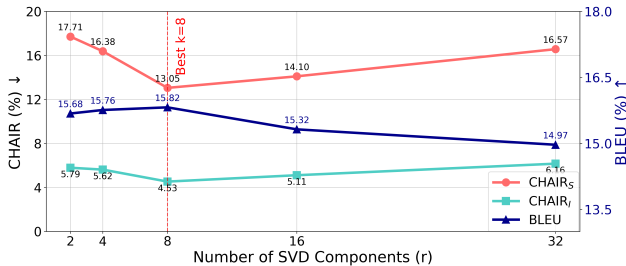


Figure 8. Ablation study on subspace rank (r)

forward corruption and reverse denoising conditioned on a hallucinated caption, using Equation 2 and Equation 3, respectively. This produces images with increasing semantic shift. We compute hidden-state differences between hallucinated and original pairs, apply SVD to extract the hallucination subspace, and use it for test-time projection. As shown in Figure 7, the subspace from $t_h = 0.5T$ achieves the best CHAIR_S. We attribute this to intermediate steps yielding structurally faithful yet semantically altered images, striking a balance that best isolates hallucination directions.

Effect of Subspace Rank. We study how the number of singular vectors (r) used to define the hallucination subspace affects performance. For the LLaVA-7B model, we sweep $r \in \{2, 4, 8, 16, 32\}$ and evaluate on the CHAIR benchmark. As shown in Figure 8, $r = 8$ yields the best results: CHAIR_S and CHAIR_I are minimized, while BLEU reaches its peak, indicating improved faithfulness and fluency. Further component-selection results for MiniGPT-4 and mPLUG-Owl2 are given in the Appendix.

Robustness to Visual Noise. To evaluate the robustness of our method under degraded visual inputs, we corrupt test images with varying levels of Gaussian noise ($\sigma \in$

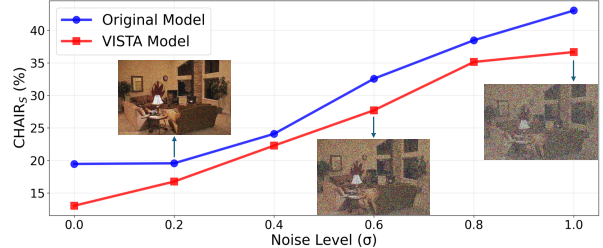


Figure 9. CHAIR_S of the original and CIPHER-refined models under increasing levels of Gaussian noise.

$\{0.0, 0.2, 0.4, 0.6, 0.8, 1.0\}$) and measure CHAIR_S for both the original and CIPHER-refined models. As shown in Figure 9, hallucination rates increase with noise for both models, but CIPHER consistently achieves lower CHAIR_S scores at all levels. The gap widens under severe noise, highlighting CIPHER’s resilience to visual degradation and its strong generalization in suppressing hallucinations.

Effect of Hallucination Source. To assess the contribution of each modality to hallucination suppression, we construct the hallucination subspace under three settings: (1) text-only hallucination using GPT, (2) image-only hallucination via Stable Diffusion, and (3) joint hallucination. In all cases, we compute feature differences and apply SVD to extract hallucination directions.

Text	Image	CHAIR _S ↓	CHAIR _I ↓	BLEU ↑
✓	✗	15.20	5.30	15.69
✗	✓	13.05	4.53	15.82
✓	✓	15.71	5.32	15.66

Table 5. Ablation study on the source of hallucination. ✓ denotes hallucinated input and ✗ denotes ground-truth input.

As shown in Table 5, image-only perturbation yields the lowest CHAIR scores, indicating more coherent and discriminative hallucination directions. Text-only perturbation performs moderately, while combining both slightly degrades performance.

5. Conclusion and Future Work

We presented CIPHER, a novel test-time hallucination mitigation method that suppresses vision-induced hallucinations in large vision-language models without requiring training or architectural modifications. CIPHER identifies hallucination directions by contrasting clean and perturbed representations, where perturbations are introduced via semantically altered images generated using Stable Diffusion. It then suppresses hallucinated content by projecting hidden states onto the null space of these directions, improving factual accuracy while preserving fluency. Extensive experiments across multiple benchmarks show that CIPHER consistently outperforms state-of-the-art baselines. While CIPHER currently uses a fixed offline projection, a promising future direction is to adapt the projection dynamically per input for more flexible, context-aware hallucination suppression.

References

- [1] Jean-Baptiste Alayrac, Jeff Donahue, Pauline Luc, Antoine Miech, Iain Barr, Yana Hasson, Karel Lenc, Arthur Mensch, Katherine Millican, Malcolm Reynolds, et al. Flamingo: a visual language model for few-shot learning. *Advances in neural information processing systems*, 35:23716–23736, 2022. 2
- [2] Wenbin An, Feng Tian, Sicong Leng, Jiahao Nie, Haonan Lin, QianYing Wang, Ping Chen, Xiaoqin Zhang, and Shijian Lu. Mitigating object hallucinations in large vision-language models with assembly of global and local attention. In *Proceedings of the Computer Vision and Pattern Recognition Conference*, pages 29915–29926, 2025. 3
- [3] Jiaqi Bai, Hongcheng Guo, Zhongyuan Peng, Jian Yang, Zhoujun Li, Mohan Li, and Zhihong Tian. Mitigating hallucinations in large vision-language models by adaptively constraining information flow. In *Proceedings of the AAAI Conference on Artificial Intelligence*, pages 23442–23450, 2025. 2
- [4] Zechen Bai, Pichao Wang, Tianjun Xiao, Tong He, Zongbo Han, Zheng Zhang, and Mike Zheng Shou. Hallucination of multimodal large language models: A survey. *arXiv preprint arXiv:2404.18930*, 2024. 1
- [5] Tom Brown, Benjamin Mann, Nick Ryder, Melanie Subbiah, Jared D Kaplan, Prafulla Dhariwal, Arvind Neelakantan, Pranav Shyam, Girish Sastry, Amanda Askell, et al. Language models are few-shot learners. *Advances in neural information processing systems*, 33:1877–1901, 2020. 2
- [6] Tom Brown, Benjamin Mann, Nick Ryder, Melanie Subbiah, Jared D Kaplan, Prafulla Dhariwal, Arvind Neelakantan, Pranav Shyam, Girish Sastry, Amanda Askell, et al. Language models are few-shot learners. *Advances in neural information processing systems*, 33:1877–1901, 2020. 2
- [7] Junzhe Chen, Tianshu Zhang, Shiyu Huang, Yuwei Niu, Linfeng Zhang, Lijie Wen, and Xuming Hu. Ict: Image-object cross-level trusted intervention for mitigating object hallucination in large vision-language models. In *Proceedings of the Computer Vision and Pattern Recognition Conference*, pages 4209–4221, 2025. 3
- [8] Zhe Chen, Jiannan Wu, Wenhai Wang, Weijie Su, Guo Chen, Sen Xing, Muyan Zhong, Qinglong Zhang, Xizhou Zhu, Lewei Lu, et al. Internvl: Scaling up vision foundation models and aligning for generic visual-linguistic tasks. In *Proceedings of the IEEE/CVF conference on computer vision and pattern recognition*, pages 24185–24198, 2024. 2
- [9] Zhaorun Chen, Zhuokai Zhao, Hongyin Luo, Huaxiu Yao, Bo Li, and Jiawei Zhou. Halc: Object hallucination reduction via adaptive focal-contrast decoding. *arXiv preprint arXiv:2403.00425*, 2024. 2, 4, 5, 1
- [10] Wei-Lin Chiang, Zhuohan Li, Ziqing Lin, Ying Sheng, Zhanghao Wu, Hao Zhang, Lianmin Zheng, Siyuan Zhuang, Yonghao Zhuang, Joseph E Gonzalez, et al. Vicuna: An open-source chatbot impressing gpt-4 with 90%* chatgpt quality. See <https://vicuna.lmsys.org> (accessed 14 April 2023), 2(3):6, 2023. 4
- [11] Aakanksha Chowdhery, Sharan Narang, Jacob Devlin, Maarten Bosma, Gaurav Mishra, Adam Roberts, Paul Barham, Hyung Won Chung, Charles Sutton, Sebastian Gehrmann, et al. Palm: Scaling language modeling with pathways. *Journal of Machine Learning Research*, 24(240): 1–113, 2023. 2
- [12] Yung-Sung Chuang, Yujia Xie, Hongyin Luo, Yoon Kim, James Glass, and Pengcheng He. Dola: Decoding by contrasting layers improves factuality in large language models. *arXiv preprint arXiv:2309.03883*, 2023. 5, 1
- [13] Anisha Gunjal, Jihan Yin, and Erhan Bas. Detecting and preventing hallucinations in large vision language models. In *Proceedings of the AAAI Conference on Artificial Intelligence*, pages 18135–18143, 2024. 2
- [14] Yuwei Huang et al. Opera: A decoding strategy for reducing object hallucination in llms. *arXiv preprint arXiv:2311.02460*, 2023. 2, 3, 5, 1
- [15] Fushuo Huo, Wenchao Xu, Zhong Zhang, Haozhao Wang, Zhicheng Chen, and Peilin Zhao. Self-introspective decoding: Alleviating hallucinations for large vision-language models. *arXiv preprint arXiv:2408.02032*, 2024. 2, 3
- [16] Chaoya Jiang, Haiyang Xu, Mengfan Dong, Jiaying Chen, Wei Ye, Ming Yan, Qinghao Ye, Ji Zhang, Fei Huang, and Shikun Zhang. Hallucination augmented contrastive learning for multimodal large language model. In *Proceedings of the IEEE/CVF Conference on Computer Vision and Pattern Recognition*, pages 27036–27046, 2024. 2
- [17] Sicong Leng, Hang Zhang, Guanzheng Chen, Xin Li, Shijian Lu, Chunyan Miao, and Lidong Bing. Mitigating object hallucinations in large vision-language models through visual contrastive decoding. In *Proceedings of the IEEE/CVF Conference on Computer Vision and Pattern Recognition*, pages 13872–13882, 2024. 2, 3, 5, 1
- [18] Junnan Li, Dongxu Li, Silvio Savarese, and Steven Hoi. Blip-2: Bootstrapping language-image pre-training with frozen image encoders and large language models. In *International conference on machine learning*, pages 19730–19742. PMLR, 2023. 2
- [19] Kenneth Li, Oam Patel, Fernanda Viégas, Hanspeter Pfister, and Martin Wattenberg. Inference-time intervention: Eliciting truthful answers from a language model. *Advances in Neural Information Processing Systems*, 36:41451–41530, 2023. 3
- [20] Yifan Li, Yifan Du, Kun Zhou, Jinpeng Wang, Wayne Xin Zhao, and Ji-Rong Wen. Evaluating object hallucination in large vision-language models. *arXiv preprint arXiv:2305.10355*, 2023. 5
- [21] Tsung-Yi Lin, Michael Maire, Serge Belongie, James Hays, Pietro Perona, Deva Ramanan, Piotr Dollár, and C Lawrence Zitnick. Microsoft coco: Common objects in context. In *Computer vision—ECCV 2014: 13th European conference, zurich, Switzerland, September 6–12, 2014, proceedings, part v 13*, pages 740–755. Springer, 2014. 2, 5
- [22] Fuxiao Liu, Kevin Lin, Linjie Li, Jianfeng Wang, Yaser Yacoob, and Lijuan Wang. Mitigating hallucination in large multi-modal models via robust instruction tuning. *arXiv preprint arXiv:2306.14565*, 2023. 2

- [23] Fangyu Liu et al. Lrv-instruction: A large-scale, diverse, and structured dataset for training vision-language models with less hallucination. *arXiv preprint arXiv:2309.06192*, 2023. [2](#)
- [24] Haotian Liu, Chunyuan Li, Qingyang Wu, and Yong Jae Lee. Visual instruction tuning. *Advances in neural information processing systems*, 36:34892–34916, 2023. [1](#), [2](#), [4](#)
- [25] Haotian Liu, Chunyuan Li, Yuheng Li, and Yong Jae Lee. Improved baselines with visual instruction tuning. In *Proceedings of the IEEE/CVF Conference on Computer Vision and Pattern Recognition*, pages 26296–26306, 2024. [1](#), [5](#), [6](#), [4](#)
- [26] Hanchao Liu, Wenyan Xue, Yifei Chen, Dapeng Chen, Xiutian Zhao, Ke Wang, Liping Hou, Rongjun Li, and Wei Peng. A survey on hallucination in large vision-language models. *arXiv preprint arXiv:2402.00253*, 2024. [1](#)
- [27] Sheng Liu, Haotian Ye, and James Zou. Reducing hallucinations in large vision-language models via latent space steering. In *The Thirteenth International Conference on Learning Representations*, 2025. [2](#), [3](#)
- [28] Kishore Papineni, Salim Roukos, Todd Ward, and Wei-Jing Zhu. Bleu: a method for automatic evaluation of machine translation. In *Proceedings of the 40th annual meeting of the Association for Computational Linguistics*, pages 311–318, 2002. [5](#)
- [29] Anna Rohrbach, Lisa Anne Hendricks, Kaylee Burns, Trevor Darrell, and Kate Saenko. Object hallucination in image captioning. *arXiv preprint arXiv:1809.02156*, 2018. [4](#), [5](#), [1](#)
- [30] Robin Rombach, Andreas Blattmann, Dominik Lorenz, Patrick Esser, and Björn Ommer. High-resolution image synthesis with latent diffusion models. In *Proceedings of the IEEE/CVF conference on computer vision and pattern recognition*, pages 10684–10695, 2022. [3](#)
- [31] Zhiqing Sun, Sheng Shen, Shengcao Cao, Haotian Liu, Chunyuan Li, Yikang Shen, Chuang Gan, Liangyan Gui, Yu-Xiong Wang, Yiming Yang, et al. Aligning large multimodal models with factually augmented rlhf. In *Findings of the Association for Computational Linguistics: ACL 2024*, pages 13088–13110, 2024. [5](#)
- [32] Hugo Touvron, Louis Martin, Kevin Stone, Peter Albert, Amjad Almahairi, Yasmine Babaei, Nikolay Bashlykov, Soumya Batra, Prajjwal Bhargava, Shruti Bhosale, et al. Llama 2: Open foundation and fine-tuned chat models. *arXiv preprint arXiv:2307.09288*, 2023. [2](#), [4](#)
- [33] Rheeya Uppaal, Apratim Dey, Yiting He, Yiqiao Zhong, and Junjie Hu. Model editing as a robust and denoised variant of dpo: A case study on toxicity. *arXiv preprint arXiv:2405.13967*, 2024. [3](#)
- [34] Wenyi Xiao, Ziwei Huang, Leilei Gan, Wanggui He, Haoyuan Li, Zhelun Yu, Fangxun Shu, Hao Jiang, and Linchao Zhu. Detecting and mitigating hallucination in large vision language models via fine-grained ai feedback. In *Proceedings of the AAAI Conference on Artificial Intelligence*, pages 25543–25551, 2025. [2](#)
- [35] Le Yang, Ziwei Zheng, Boxu Chen, Zhengyu Zhao, Chenhao Lin, and Chao Shen. Nullu: Mitigating object hallucinations in large vision-language models via halluspace projection. In *Proceedings of the Computer Vision and Pattern Recognition Conference*, pages 14635–14645, 2025. [2](#), [3](#), [4](#), [5](#), [1](#)
- [36] Tianyun Yang, Ziniu Li, Juan Cao, and Chang Xu. Mitigating hallucination in large vision-language models via modular attribution and intervention. In *Adaptive Foundation Models: Evolving AI for Personalized and Efficient Learning*, 2025. [3](#)
- [37] Zhihe Yang, Xufang Luo, Dongqi Han, Yunjian Xu, and Dongsheng Li. Mitigating hallucinations in large vision-language models via dpo: On-policy data hold the key. In *Proceedings of the Computer Vision and Pattern Recognition Conference*, pages 10610–10620, 2025. [2](#)
- [38] Jiabo Ye, Haiyang Xu, Haowei Liu, Anwen Hu, Ming Yan, Qi Qian, Ji Zhang, Fei Huang, and Jingren Zhou. mplug-owl3: Towards long image-sequence understanding in multi-modal large language models. *arXiv preprint arXiv:2408.04840*, 2024. [1](#)
- [39] Qinghao Ye, Haiyang Xu, Jiabo Ye, Ming Yan, Anwen Hu, Haowei Liu, Qi Qian, Ji Zhang, and Fei Huang. mplug-owl2: Revolutionizing multi-modal large language model with modality collaboration. In *Proceedings of the IEEE/CVF conference on computer vision and pattern recognition*, pages 13040–13051, 2024. [1](#), [2](#), [4](#)
- [40] Shukang Yin, Chaoyou Fu, Sirui Zhao, Tong Xu, Hao Wang, Dianbo Sui, Yunhang Shen, Ke Li, Xing Sun, and Enhong Chen. Woodpecker: Hallucination correction for multimodal large language models. *Science China Information Sciences*, 67(12):220105, 2024. [2](#), [5](#)
- [41] Haoxuan You, Haotian Zhang, Zhe Gan, Xianzhi Du, Bowen Zhang, Zirui Wang, Liangliang Cao, Shih-Fu Chang, and Yinfei Yang. Ferret: Refer and ground anything anywhere at any granularity. *arXiv preprint arXiv:2310.07704*, 2023. [2](#)
- [42] Yiyang Zhou, Chenhang Cui, Jaehong Yoon, Linjun Zhang, Zhun Deng, Chelsea Finn, Mohit Bansal, and Huaxiu Yao. Analyzing and mitigating object hallucination in large vision-language models. *arXiv preprint arXiv:2310.00754*, 2023. [2](#), [3](#), [5](#)
- [43] Deyao Zhu, Jun Chen, Xiaoqian Shen, Xiang Li, and Mohamed Elhoseiny. Minigt-4: Enhancing vision-language understanding with advanced large language models. *arXiv preprint arXiv:2304.10592*, 2023. [1](#), [2](#), [4](#)
- [44] Lanyun Zhu, Deyi Ji, Tianrun Chen, Peng Xu, Jieping Ye, and Jun Liu. Ibd: Alleviating hallucinations in large vision-language models via image-biased decoding. In *Proceedings of the Computer Vision and Pattern Recognition Conference*, pages 1624–1633, 2025. [3](#)

6. Implementation Details

Table 6 summarizes the general and model-specific parameters used in our experiments. We adopt a deterministic decoding setup with fixed temperature and beam size, and vary the maximum number of generated tokens depending on the evaluation benchmark.

To simulate visual hallucinations, we use Stable Diffusion with half of total diffusion steps (T) for forward and reverse steps ($0.5T$). During inference, hidden representations from selected layers are projected onto the orthogonal complement of the hallucination subspace. The rank of this subspace is tuned for each model to optimize hallucination suppression without compromising generation quality.

Parameters	Values
General Settings	
Temperature	0
Number of Beams	3
Maximum New Tokens (CHAIR)	64
Maximum New Tokens (OPOPE)	256
Maximum New Tokens (LLaVA-Bench)	1024
Number of Diffusion Steps	$0.5T$
Editing Layers	16-32
Model-Specific Parameters	
Hallucination Space Rank (LLaVA-1.5)	8
Hallucination Space Rank (MiniGPT-4)	64
Hallucination Space Rank (mPLUG-Owl2)	32

Table 6. General and model-specific parameter settings.

We report the performance of baseline models based on the results presented in the Nullu paper [35], which reproduces several state-of-the-art object hallucination mitigation methods, including HALC [9], VCD [17], DoLa [12], and OPERA [14]. Each method is evaluated using its official implementation and publicly released pre-trained checkpoints. Moreover, we carefully adopted key hyperparameter settings that align with those reported in their original implementations. Specifically, for HALC, we used an amplification factor of 0.05 along with a beam size of 1, reflecting the minimal decoding augmentation strategy employed by the authors. For VCD, we set the diffusion noise step to 500, consistent with the level of perturbation used in their hallucination mitigation framework. In the case of DoLa, we applied a repetition penalty of 1.2 and performed interventions across the early transformer layers, as suggested to promote faithful generation during early stages of decoding. Lastly, for OPERA, we implemented a scaled self-attention mechanism with a scaling factor of 50, in line with the original design to regulate attention intensity. All these hyperparameter choices were selected to faithfully reproduce the respective baselines under settings that remain true to the original authors’ reported configurations.

7. Detailed Results for OPOPE

To evaluate the effectiveness of hallucination mitigation methods in a way that is compatible with post-hoc approaches, we adopt the Offline POPE (OPOPE) protocol. OPOPE is a non-interactive version of the original POPE metric, introduced in HALC [9], and is specifically designed to avoid the limitations of online interaction during inference. While POPE evaluates hallucination through interactive polling prompts such as “Is there a/an [object] in the image?”, this interactive requirement poses challenges for post-hoc mitigation methods and can lead to instability in models with weaker generative backbones.

OPOPE performs hallucination evaluation entirely offline. Following the caption generation pipeline of CHAIR [29], captions are generated for a fixed image set, then tokenized and singularized, with words mapped to MSCOCO object categories using synonym and compound-word mappings. Using POPE’s sampling strategy, three test object lists are created per setting—*Random*, *Popular*, and *Adversarial*—each containing six objects balanced between ground-truth and nonexistent categories. Captions are scanned for these objects, and mentions of nonexistent ones are counted as hallucinations.

To account for the limited recall sensitivity of offline evaluations—where false negatives may occur if hallucinated content is not explicitly verbalized—we adopt the F_β score as our primary evaluation metric, following HALC. The F_β score reduces the penalty on false negatives by weighting precision more heavily. Specifically, we use $\beta = 0.2$ for F_β score:

$$F_\beta = \frac{(1 + \beta^2) \cdot (\text{precision} \cdot \text{recall})}{\beta^2 \cdot \text{precision} + \text{recall}} \quad \text{with } \beta = 0.2.$$

The main paper reports results averaged across the three sampling strategies for brevity, while Table 7 provides a full breakdown by model and sampling configuration. We report Accuracy, Precision, Recall, and F-score for all baselines—Greedy, Beam Search, DoLa [12], OPERA [14], VCD [17], HALC [9], and NullU [35]—along with our method, VISTA. VISTA consistently ranks among the top-performing methods across most settings, demonstrating robustness to varying object distributions and model architectures. These results complement the main findings and provide a detailed view of performance under each hallucination sampling strategy.

We additionally conducted statistical significance tests comparing VISTA to baseline methods for each model. Across all cases, results consistently showed significant improvements. For instance, on LLaVA, VISTA outperforms the baseline with p-values well below 0.01 across all metrics: Accuracy ($p = 0.0033$), Precision ($p < 0.0001$), and $F_{0.2}$ Score ($p < 0.0001$), confirming the robustness of our method.

Setting	Model	Method	Accuracy	Precision	Recall	F Score
Random	LLaVA-1.5	Greedy	81.52	98.41	64.07	96.42
		DoLa	81.38	98.11	64.00	96.14
		OPERA	81.62	98.57	64.17	96.58
		VCD	80.57	98.41	62.13	96.25
		HALC	79.58	98.21	60.27	95.89
		Nullu	81.18	98.05	63.63	96.05
		VISTA	81.84	98.70	64.58	96.68
	MiniGPT-4	Greedy	72.42	98.49	45.53	94.25
		DoLa	72.45	98.58	45.57	94.34
		OPERA	72.57	98.78	45.70	94.52
		VCD	72.35	98.19	45.53	93.97
		HALC	72.08	98.62	44.80	94.25
		Nullu	72.68	99.06	45.80	94.82
		VISTA	72.85	99.37	46.00	95.12
	mPLUG-Owl2	Greedy	79.45	97.74	60.30	95.46
		DoLa	78.33	97.60	58.10	95.09
		OPERA	78.31	97.73	57.96	95.21
		VCD	78.19	98.23	57.42	95.61
		HALC	77.83	97.72	57.00	95.10
		Nullu	79.05	98.40	60.50	95.82
		VISTA	79.56	97.66	60.57	95.41
Popular	LLaVA-1.5	Greedy	78.93	91.17	64.07	89.71
		DoLa	78.72	91.60	64.00	89.26
		OPERA	79.22	91.80	64.17	90.30
		VCD	77.57	89.87	62.13	88.35
		HALC	77.47	91.87	60.27	90.05
		Nullu	79.80	94.06	63.63	92.36
		VISTA	80.02	93.47	64.58	91.89
	MiniGPT-4	Greedy	70.80	92.01	45.53	88.53
		DoLa	70.90	92.33	45.57	88.22
		OPERA	71.10	92.82	45.70	89.27
		VCD	70.33	90.30	45.53	86.98
		HALC	70.92	93.80	44.80	90.00
		Nullu	71.97	96.08	45.80	92.19
		VISTA	72.15	96.43	46.00	92.53
	mPLUG-Owl2	Greedy	76.00	87.90	60.30	86.38
		DoLa	75.20	88.36	58.10	86.00
		OPERA	75.02	88.06	57.96	86.33
		VCD	74.86	88.16	57.42	86.37
		HALC	75.77	91.34	57.00	89.26
		Nullu	77.09	92.34	61.60	90.49
		VISTA	77.95	92.91	60.57	91.03
Adversarial	LLaVA-1.5	Greedy	76.97	86.36	64.07	85.22
		DoLa	76.85	86.18	64.00	85.05
		OPERA	77.03	86.40	64.17	85.26
		VCD	75.88	85.71	62.13	84.48
		HALC	76.57	89.44	60.27	87.80
		Nullu	77.58	88.27	63.63	86.92
		VISTA	78.29	89.03	64.58	87.84
	MiniGPT-4	Greedy	70.43	90.65	45.53	87.32
		DoLa	70.50	88.55	45.57	87.50
		OPERA	70.78	91.63	45.70	88.21
		VCD	69.82	83.41	45.53	85.32
		HALC	70.52	92.22	44.80	88.60
		Nullu	71.10	92.73	45.80	89.21
		VISTA	71.44	93.70	46.00	90.11
	mPLUG-Owl2	Greedy	74.23	83.58	60.30	82.36
		DoLa	73.52	83.98	58.10	82.55
		OPERA	73.17	83.45	57.96	82.06
		VCD	72.85	83.01	57.42	81.61
		HALC	74.02	86.41	57.00	84.72
		Nullu	75.15	87.76	61.60	86.10
		VISTA	76.10	87.90	60.57	86.40

Table 7. Performance comparison of various hallucination mitigation methods across different models and evaluation settings.

Examples of Hallucinated Images

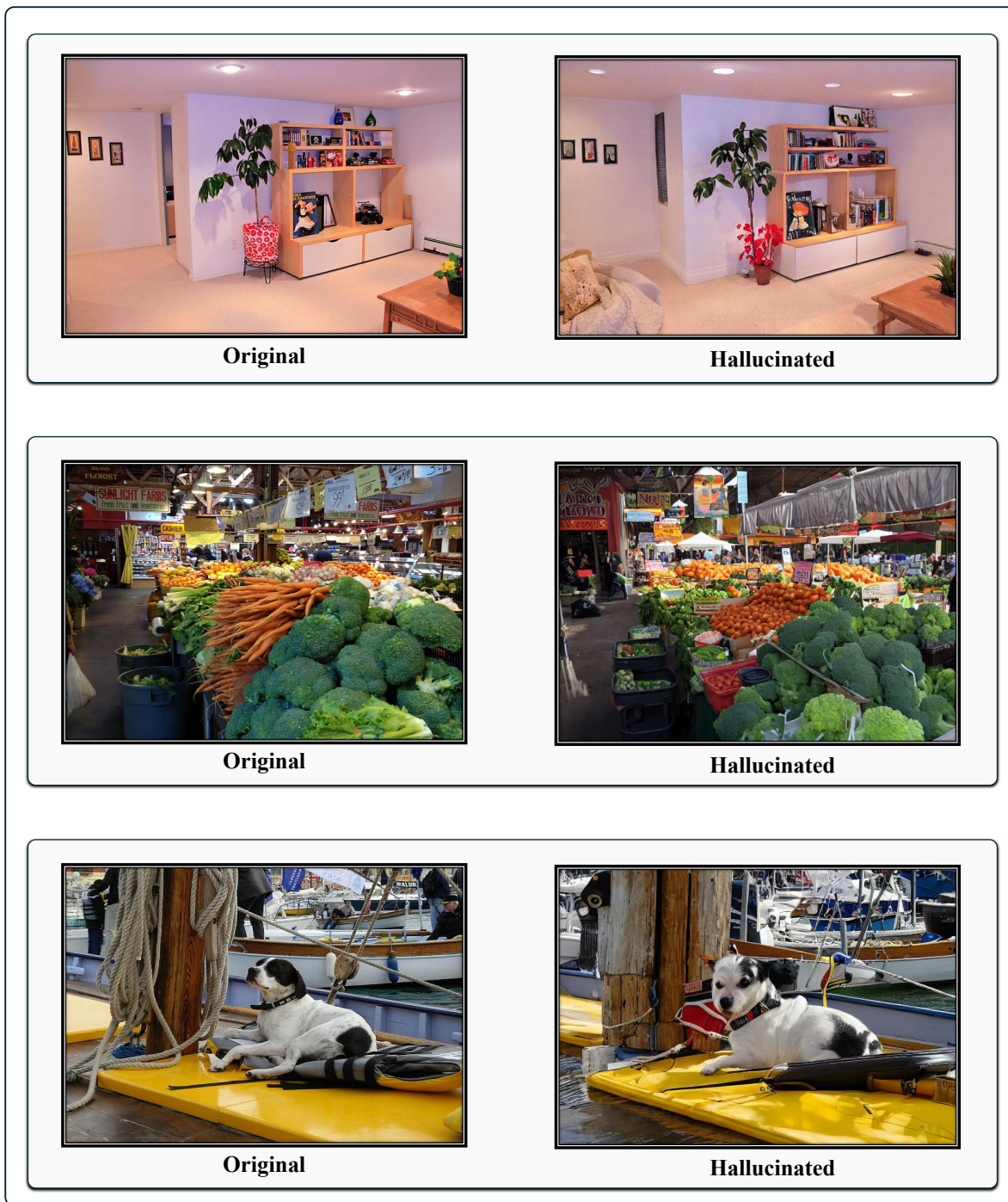


Figure 10. Visual examples from the MSCOCO dataset illustrating hallucinations generated using $0.5T$ Stable Diffusion steps.

This figure shows MSCOCO images before and after applying visual hallucination using Stable Diffusion with $t_h = 0.5T$ denoising steps. While the overall scene struc-

ture remains largely unchanged, the hallucinated images introduce subtle object or texture modifications intended to mislead vision-language models.

8. Extended Ablation Analysis

In this section of the appendix, we provide extended results from our ablation analysis to support the findings presented in the main paper.

8.1. Best Subspace Rank

As shown in the ablation section of the main paper, the best subspace rank for LLaVA-7B was $r = 8$, achieving the lowest CHAIR_S and CHAIR_I scores while preserving or improving BLEU. Here, we extend this analysis to MiniGPT-4 and mPLUG-Owl2.

Figure 11 shows that for MiniGPT-4, the optimal number of SVD components is $r = 64$, where CHAIR scores drop significantly and BLEU remains stable. Similarly, Figure 12 demonstrates that mPLUG-Owl2 achieves the best balance at $r = 32$, where hallucination metrics are minimized and BLEU degradation is minimal. These findings highlight that the optimal subspace rank can vary across models and should be tuned accordingly.

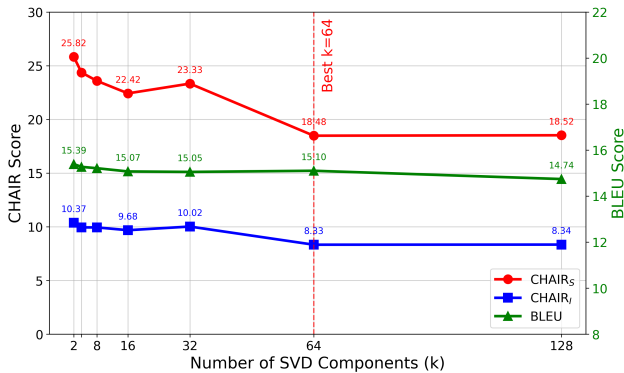


Figure 11. Effect of subspace rank r on CHAIR_S, CHAIR_I, and BLEU for MiniGPT-4 on the CHAIR benchmark. Using $r = 64$ yields the best performance, minimizing hallucinations with minimum BLEU degradation.

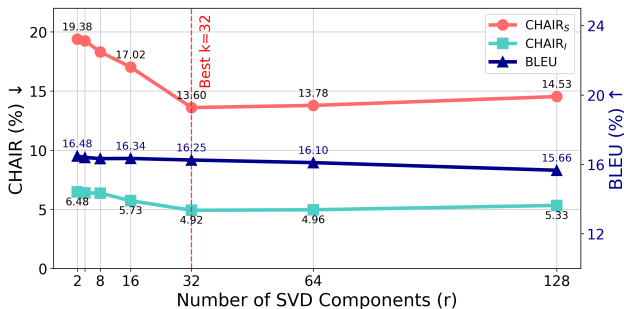


Figure 12. Effect of subspace rank r on CHAIR_S, CHAIR_I, and BLEU for mPLUG-Owl2 on the CHAIR benchmark. Using $r = 32$ yields the best performance, minimizing hallucinations with minimum BLEU degradation.

8.2. Selection of Layers for Projection

VISTA mitigates hallucinations at inference time by projecting the hidden representations of selected LVLM layers onto their corresponding null spaces. To assess the influence of layer choice on suppression effectiveness, we perform an ablation study using various candidate layer ranges. We evaluate each configuration on the MSCOCO validation split using the CHAIR metric, reporting both instance-level (CHAIR_I) and sentence-level (CHAIR_S) hallucination rates, where lower values indicate better suppression.

Layer Range	CHAIR _S ↓	CHAIR _I ↓
8–16	13.52	4.82
8–24	14.10	5.02
16–24	18.10	5.86
16–32	13.05	4.53
20–32	14.10	4.84
24–32	14.00	4.64
28–32	14.48	5.10

Table 8. Ablation study on the transformer layer range used for projection in VISTA.

As shown in Table 8, the choice of layer range significantly impacts hallucination suppression. Projection over earlier layers, such as 8–16 or narrower bands like 28–32, yields suboptimal results, suggesting that local or overly shallow representations lack the semantic expressiveness needed to isolate hallucination directions. Performance improves with broader and deeper projections, with the 16–32 range consistently achieving the lowest CHAIR_S and CHAIR_I scores. This indicates that hallucination-inducing signals are best captured in semantically rich, higher layers spanning a sufficiently deep interval. Consequently, we adopt the 16–32 layer range as the default configuration in our main experiments.

9. Details of GPT-4V Aided Evaluation on LLaVA-Bench

We evaluate our hallucination suppression method using GPT-4V on the LLaVA-Bench benchmark [25], which consists of 24 images. For each example, GPT-4V receives the image, the evaluation prompt, and the responses from both the original and the edited (hallucination-suppressed) models.

GPT-4V compares the two responses in terms of accuracy—how well the answer reflects the image—and detailedness—how specific and complete the response is. It outputs a score for each criterion along with a brief justification. Figure 13 and Figure 14 show the prompt format and a sample GPT-4V evaluation, respectively. This setup enables consistent comparison of response quality grounded in the image content.

Prompt for GPT-4V Aided Evaluation

Descriptions:

AI that scores image description accuracy and detailedness.

Instructions:

You are an AI designed to evaluate and score the performance of two AI assistants in describing a given image. Your primary focus is on the accuracy and detailedness of their descriptions. You will assess the accuracy by checking for hallucinations - any part of the description that is inconsistent with the image content. For detailedness, you will consider how rich the response is in necessary details, excluding any hallucinated parts. You will provide scores on a scale from 1 to 10 for each assistant separately, based on these criteria. After scoring, you will offer an explanation for your evaluation, ensuring it is free from bias and not influenced by the order of presentation of the responses.

Input format:

[Assistant1]
{Response1}
[End of Assistant1]

[Assistant2]
{Response2}
[End of Assistant2]

Output format:

Accuracy:

- Assistant1: [score]/10
- Assistant2: [score]/10
- Reason: [explanation for accuracy scores]

Detailedness:

- Assistant1: [score]/10
- Assistant2: [score]/10
- Reason: [explanation for detailedness scores]

Figure 13. An illustration of the prompt used to guide GPT-4V for visual question evaluation.

Input:



[Assistant1]

The image features two large subway sandwiches, each cut in half, placed on a black background. The sandwiches are filled with various ingredients, including lettuce, tomatoes, and cheese. The sandwiches are positioned close to each other, creating a visually appealing presentation. The close-up view of the sandwiches highlights their delicious and appetizing appearance.

[End of Assistant1]

[Assistant2]

The image features a close-up view of a Subway Series sandwich, showcasing its delicious ingredients. The sandwich is filled with a generous amount of meat, lettuce, and cheese, making it a mouth-watering meal. The Subway Series logo is also visible in the background, emphasizing the brand's commitment to quality and taste. The sandwich is presented on a black background, allowing the viewer to focus solely on the appetizing details of the meal.

[End of Assistant2]

GPT-4V Output:

Accuracy:

- Assistant1: 8/10
- Assistant2: 9/10

- **Reason:** Assistant1 accurately describes the presence of sandwiches and their ingredients but incorrectly mentions that the sandwiches are cut in half, which is not visible in the image. Assistant2 accurately describes the sandwich and includes the presence of the Subway Series logo, which is visible in the image, making it slightly more accurate.

Detailedness:

- Assistant1: 7/10
- Assistant2: 8/10

- **Reason:** Assistant1 provides a good level of detail about the ingredients and presentation but lacks mention of the Subway Series logo, which is a significant detail. Assistant2 includes details about the ingredients and the logo, adding to the richness of the description. However, it could have included more specifics about the ingredients visible, such as the presence of onions.

Figure 14. Example of GPT-4V-based evaluation for image description.

More Examples of VISTA on LLaVA-Bench



Prompt: please describe this image in detail.

Original Model: The image features a small brown dog lying on a wooden floor, possibly a porch or a deck. The dog appears to be sleeping or resting, taking up a significant portion of the floor. The scene is set on a blue surface, which adds a contrasting color to the image. In the background, there is a chair placed near the left edge of the image, and a dining table can be seen in the upper left corner. The overall atmosphere of the scene is relaxed and peaceful, with the dog enjoying its time on the floor.

VISTA: The image features a small, cute French Bulldog laying down on a blue hardwood floor. The dog appears to be sleeping or resting comfortably, occupying a significant portion of the floor's space. In the background, there is a chair positioned on the left side of the scene. The overall atmosphere of the scene is cozy and inviting.



Prompt: please describe this image in detail.

Original Model: The image features a young boy wearing glasses and a bow tie, standing in front of a building. He appears to be smiling and posing for the camera. The boy is wearing a blue suit and a red bow tie, giving him a formal and stylish appearance. The scene is set in a city environment, with a backdrop of buildings and a street visible in the background.

VISTA: The image features a young boy wearing a red bow tie and a blue jacket. He appears to be the main focus of the scene. The boy is also wearing eyeglasses, which adds a distinctive touch to his outfit. In the background, there are a few other people present, but they do not seem to be the main subject of the image. The boy's outfit creates a lively atmosphere.



Prompt: please describe this image in detail.

Original Model: The image features a wooden table with a basket of fruit, including a variety of fruits such as apples, oranges, and bananas. There are three apples on the table, with one placed near the left side, another in the middle, and the third one on the right side. In addition to the apples, there are three oranges on the table. One orange is located on the left side, another one is in the middle, and the third one is on the right side. A banana can also be seen on the table, positioned towards the right side. The table appears to be a dining table, and the fruits are arranged neatly on it.

VISTA: The image features a close-up view of a group of four unripe, dark-colored fruits. The fruits are placed on a dining table, with one of them being sliced open to reveal the inside. The sliced fruit is located in the center of the image, while the other three fruits are positioned around it. In addition to the fruits, there is a basket present in the scene, which is located at the top-left corner of the image. The presence of the basket suggests that the fruits may have been recently harvested or are being displayed for sale or consumption.

Figure 15. More examples of VISTA applied to LLaVA-Bench.